Supplementary Information for

Decadal Trends in the Ocean Carbon Sink

Tim DeVries, Corinne Le Quéré, Oliver Andrews, Sarah Berthet, Judith Hauck, Tatiana Ilyina, Peter Landshutzer, Andrew Lenton, Ivan Lima, Michael Nowicki, Jörg Schwinger, and Roland Séférian

Tim DeVries.
E-mail: tdevries@geog.ucsb.edu

This PDF file includes:

Supplementary text
Figs. S1 to S3
Table S1
References for SI reference citations

www.pnas.org/cgi/doi/10.1073/pnas.1900371116

Supporting Information Text

SI Methods. This Appendix provides additional information on the models and methods used in this study.

pCO$_2$-based flux mapping products. We used a subset of the SOCOM models that capture climate-driven variability in the ocean CO_2 sink over at least two decades (1, 2): UEA-SI (3), Jena-MLS (4), CU-SCSE (2), AOML-EMP (5), JMA-MLR (6), ETH-SOMFFN (7), CARBONES-NN (2), NIES-NN (8), and PU-MCMC (9). The reader is referred to ref. (2) for further details on the methods used by each of these models.

Inverse models (OCIM). The two different OCIM versions capture the effects of different processes on ocean CO_2 uptake. The OCIM with steady circulation (OCIM-steady) (10) does not capture variability in circulation, biology, or solubility, and does not simulate the cycling of "natural" (pre-anthropogenic) CO_2 in the ocean. Error estimates are derived from the 10 different versions of the model that vary in terms of their sub-gridscale diffusivities and incorporation of observational errors as described in ref. (10). The OCIM with decadal variations in ocean circulation (OCIM-variable) (11) captures variability in the natural and anthropogenic CO_2 fluxes due to ocean circulation variability, but does not resolve variability due to solubility or biology. The influence of solubility changes is small on decadal timescales as demonstrated by ref. (11), but the effect of changes in biologically-driven CO_2 uptake is unknown. Error estimates are derived from 160 different versions of the model that vary in terms of their physical and biogeochemical parameters as described in ref. (11).

Global ocean biogeochemistry models (GOBMs). As mentioned in the Materials and Methods, each modeling group performed three simulations for this study. The first is the Global Carbon Budget 2017 (GCB17) simulation (12), which uses reanalysis climate forcing and observed atmospheric CO_2 concentrations (simulation A: "CO_2+climate") from 1959-2017. "Climate forcing" in this case refers to wind stress and surface heat and freshwater fluxes diagnosed from re-analysis products (see **Table S1**). The second simulation uses constant climate forcing and atmospheric CO_2 (simulation B: "constant climate and CO_2"). The third simulation uses constant climate forcing and observed atmospheric CO_2 concentrations 1959-2017 (simulation C: "constant climate and increasing CO_2"). Using these runs we defined the oceanic CO_2 uptake due to both climate and CO_2 variability (simulation A:"CO_2+climate"), the CO_2 uptake due to atmospheric CO_2 variability alone (simulation C − simulation B: "CO_2 only"), and the CO_2 uptake due to climate variability alone (simulation A − simulation C: "climate only"). We did not correct for model drift, but we did verify that the model drift (from run B) has a negligible influence on the decadal trends reported here.

The simulations run by each group differed slightly in terms of their model spin-up procedure, their choice of climatological forcing for the "constant climate" run, and their choice of historical climate forcing for the variable-climate runs. These differences are summarized in **Table S1**. All groups used the observed atmospheric CO_2 concentrations from the GCB17 (12) for simulations A and C, and a constant atmospheric pCO_2 from 1959 for simulation B.

Dynamic global vegetation models (DGVMs). The DGVMs used here are the same as those appearing in the 2017 Global Carbon Budget: CABLE (13). CLASS-CTEM (14), CLM4.5 (15), DLEM (16), ISAM (17), JSBACH (18), JULES (19), LPJ-GUESS (20), LPJ (21), LPX-Bern (22), OCN (23), ORCHIDEE (24), ORCHIDEE-MICT (25), SDGVM (26), and VISIT (27).

Definitions of ocean regions. For Figures 3, 4, S2, and S3 we calculated regional decadal trends by integrating fluxes over distinct oceanographic regions. These regions are based on time-mean open-ocean biomes defined by sea-surface temperature, chlorophyll concentrations, ice fraction, and mixed layer depth (28). The regions used here correspond to the biomes define by ref. (28) as follows: "Southern Ocean" is the union of the Southern Ocean sub-tropical seasonally stratified biome, the Southern Ocean sub-polar seasonally-stratified biome, and the Southern Ocean ice biome. "North Atlantic" is the union of the North Atlantic sub-polar seasonally-stratified biome and the North Atlantic sub-tropical seasonally-stratified biome. "North Pacific" is the union of the North Pacific sub-polar seasonally-stratified biome and the North Pacific sub-tropical seasonally-stratified biome. "Low-latitude Atlantic" is the union of the North Atlantic sub-tropical permanently stratified biome, the Atlantic equatorial biome and the South Atlantic sub-tropical permanently stratified biome. "Low-latitude Pacific + Indian" is the union of the North Pacific sub-tropical permanently stratified biome, the Pacific equatorial western biome, the Pacific equatorial eastern biome, the South Pacific sub-tropical permanently stratified biome, and the Indian sub-tropical permanently stratified biome. We used the SOCOM air-sea CO_2 fluxes that are available pre-computed on these regions from http://www.bgc-jena.mpg.de/SOCOM/.

Structural uncertainties of the ocean CO_2 sink estimates. All of the methods for estimating the oceanic CO_2 sink have structural errors that affect their results. The primary sources of structural uncertainty in the SOCOM products are the choice of mapping methodology, as well as a lack of data from winter seasons in the high latitudes with which to constrain the air-sea fluxes in those regions. The main source of structural error in the OCIM is unresolved sub-decadal variability, which combined with the sparse hydrographic data used to constrain the model could lead to substantial aliasing effects, with potentially large impacts on the magnitude of decadal variability in ocean CO_2 uptake. The OCIM also neglects changes in biologically-driven CO_2 uptake, which could counteract the circulation-forced CO_2 variability. Structural sources of error associated with the GOBMs include parameterizations of unresolved model physics such as subgridscale ocean eddies, parameterizations of carbon cycling in marine ecosystems and biogeochemistry (which vary widely across different models (29)), and uncertainties in the climate forcing datasets used as boundary conditions for the models.

Future work should focus on alleviating these structural uncertainties in the various methods. We suggest that for the SOCOM pCO_2-based flux mapping products, the incorporation of data from ocean biogeochemical floats that can sample year-round, along with improved statistical methods for correcting for the aliasing effects resulting from seasonally-biased observations, could significantly improve their fidelity. For the OCIM method, there is a critical need to resolve sub-decadal (i.e. seasonal to interannual) variability in ocean circulation in order to avoid aliasing effects introduced during the assimilation, and to avoid unrealistic discontinuities in air-sea CO_2 fluxes introduced by the abrupt circulations changes at the decadal transitions. For the GOBMs, work should focus on identifying the most accurate historical climate forcing data, quantifying the physical and biological contributions to climate-driven changes in ocean CO_2 uptake, establishing the proper spin-up procedure for model simulations, and quantifying the sensitivity of the modeled ocean CO_2 sink to climate drivers such as wind stress and buoyancy fluxes. This work should help to identify the factors contributing to the muted variability of the GOBMs compared to the observations.

Evaluation of global ocean biogeochemistry models. Although a thorough evaluation of the GOBMs used here is beyond the scope of the present study, we provide some additional analysis of the GOBM results in order to demonstrate the differences among the various models, and to provide a comparison to high-fidelity pCO_2-based reconstructions. **Fig. S1** compares the global and regional interannual variability of the GOBMs to results from two of the SOCOM pCO_2-based flux mapping products: the Jena-MLS (4) and the ETH-SOMFFN (7). These products were identified by the SOCOM analysis as the ones that best match the interannual variability of the pCO_2 observations (2). At a global scale, we see that the models CSIRO, NorESM, MITgcm-REcoM-JRA, and NEMO-PlankTOM5 have the best agreement (r>0.6) with the interannual variability in air-sea CO_2 fluxes diagnosed by the ETH-SOMFFN product. The three regions with the greatest decadal variability in the ocean CO_2 sink are the Southern Ocean, North Pacific, and low-latitude Pacific+Indian, and so model performance is most critical in these regions. In the Southern Ocean, the NEMO-PISCES (CNRM) model performs best ($r = 0.56$), and also demonstrates the largest decadal variability of any of the GOBMs (see **Fig. 3b**). In the North Pacific, the NorESM model performs the best ($r = 0.62$) and also has the largest decadal variability of any of the GOBMs (see **Fig. 3d**). In the low-latitude Indian+Pacific ocean, the MITgcm-REcoM-JRA and CSIRO models perform noticeably better than the other models, and also display the largest decadal variability of the GOBMs (see **Fig. 3f**). Clearly, the models at capturing the regional interannual variability best also demonstrate the largest regional decadal variability.

We also examined Hovmöller diagrams for the zonally-integrated CO_2 fluxes anomalies due to climate variability in each of the GOBMs (**Fig. S1**). These were calculated by first isolating the CO_2 fluxes due to climate variability by subtracting the air-sea CO_2 fluxes of run C ("constant climate and increasing CO_2") from the air-sea CO_2 fluxes of run A ("CO_2+climate"). The resulting air-sea fluxes at each model grid point were corrected by subtracting the 30-year mean air-sea CO_2 flux over the period 1985-2015, like in ref. (30). Here we focus on the Pacific Ocean and Southern Ocean regions as these are the most important for decadal variability. These results can be compared to similar diagrams that demonstrated large decadal variations in air-sea CO_2 fluxes in the ETH-SOMFFN pCO_2-based flux mapping product (30), although we should also note that the ETH-SOMFFN results include the influence of atmospheric pCO_2 variability, whereas here we have just focussed on the climate-driven variability. The first thing to note is that none of the models show the same degree of decadal variability as that demonstrated by the ETH-SOMFFN product (30). However, in the Southern Ocean the NEMO-PISCES (CNRM) model is the one that best captures the decadal variability demonstrated by the ETH-SOMFFN. In the Equatorial Pacific, the CSIRO and CCSM-BEC models best capture the patterns of interannual variability demonstrated by the ETH-SOMFFN. Differences between the climate forcing products also become clear in the equatorial Pacific, where the MITgcm-REcoM with JRA forcing captures the interannual variability in air-sea CO_2 fluxes much better than the MITgcm-REcoM with NCEP forcing. In the North Pacific the NorESM comes closest to matching the patterns of decadal variability demonstrated by the ETH-SOMFFN. Further analysis is needed to explain the driving forces behind these patterns and the reasons for the muted variability in the models compared to the observation-based flux products.

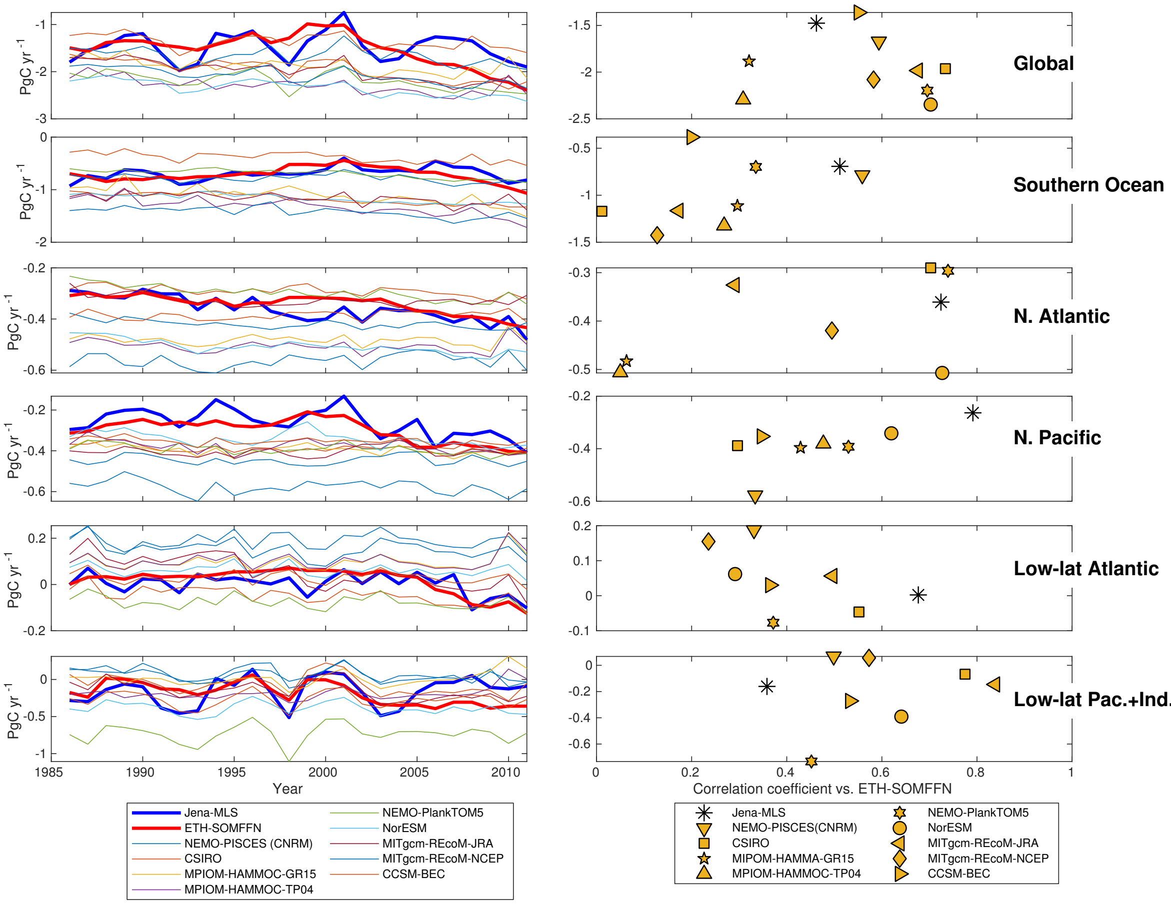

Fig. S1. (Left column) Interannual variability of the regionally-integrated air-sea CO_2 fluxes from the GOBMs used here, and two of the pCO_2-based flux products (ETH-SOMFFN (7) and Jena-MLS (4)) that best match the interannual variability of the pCO_2 observations (2). (Right column) Correlation of the regionally-integrated annual air-sea CO_2 fluxes predicted by the GOBMs used here, with the annual air-sea fluxes predicted by the ETH-SOMFFN (7) for the ocean regions used in Figures 3 and 4. Also shown is the correlation of the Jena-MLS air-sea CO_2 fluxes with the ETH-SOMFFN air-sea CO_2 fluxes for the same regions. The y-axis value for these plots is the mean air-sea CO_2 flux for each model for the period 1985-2015. Some models have negative correlation coefficients in some regions and are not shown here.

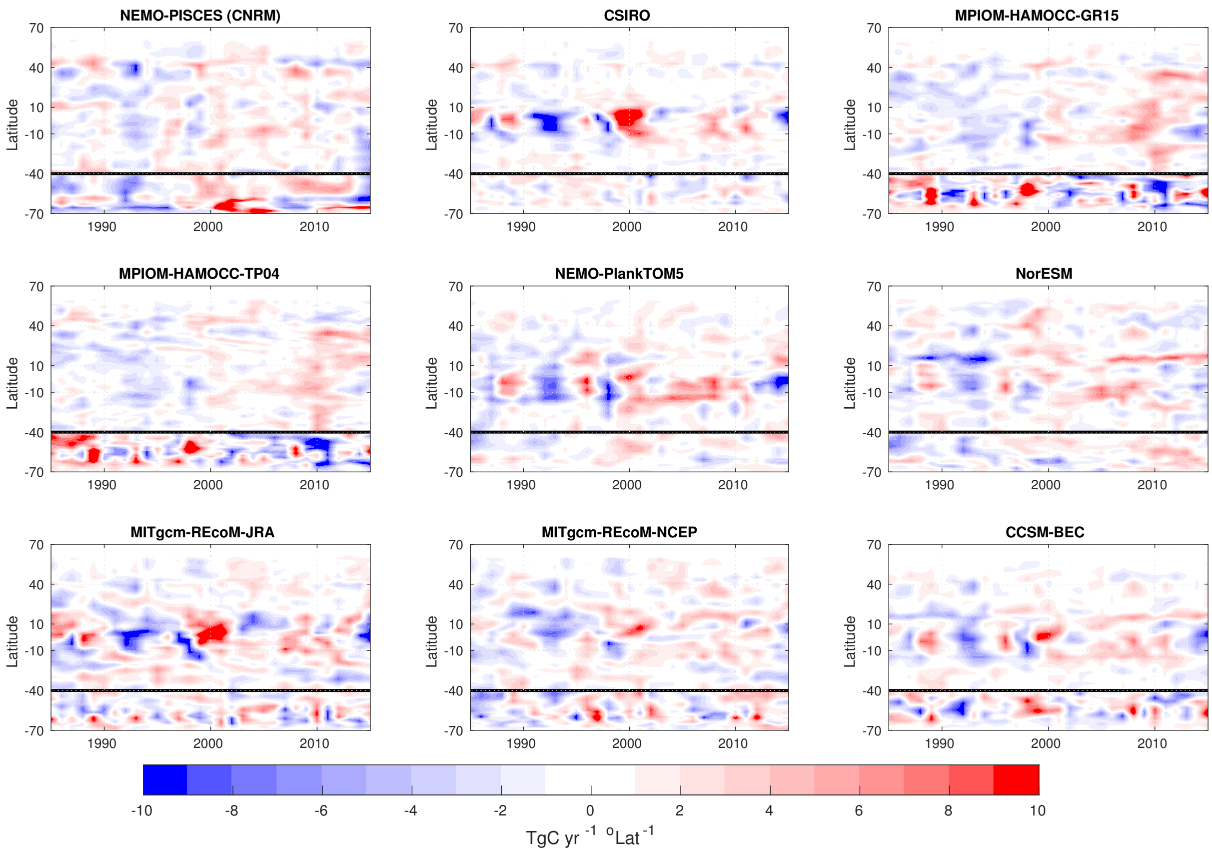

Fig. S2. Hovmöller diagrams of climate-forced variability in air-sea CO_2 fluxes for the nine GOBMs used here. The results for north of 40°S are for the Pacific Ocean, while the results south of 40°S are for the Southern Ocean (all basins). These can be compared to results for the ETH-SOMFFN discussed in ref (30) (their Figure 3).

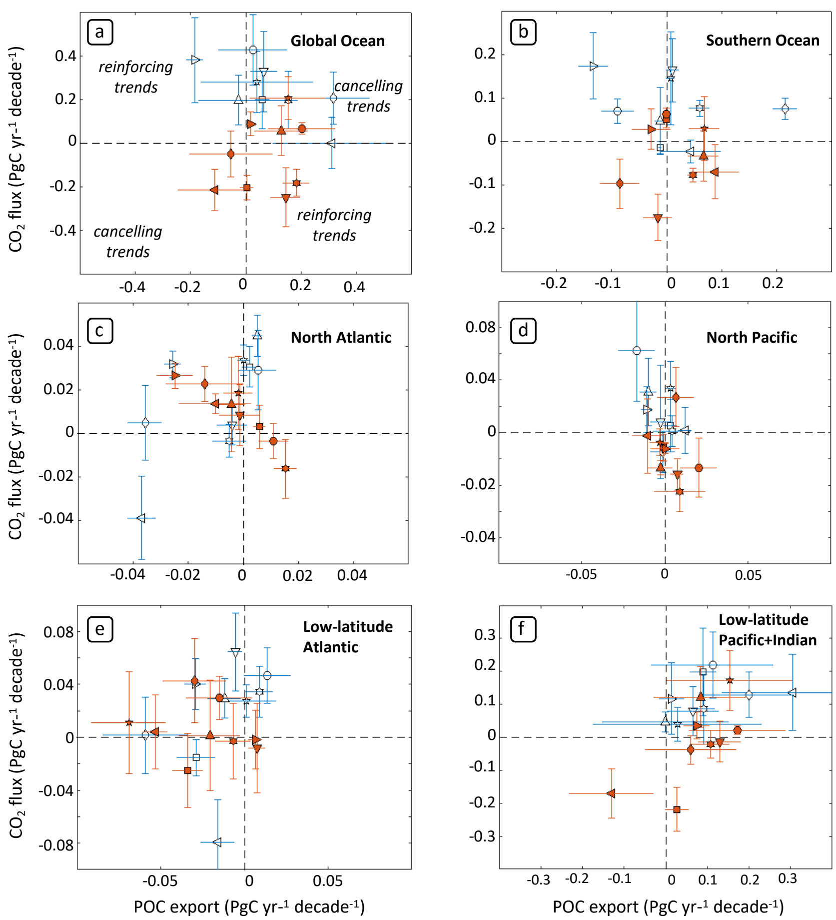

Fig. S3. Decadal trends in oceanic CO_2 uptake vs. decadal trends in POC export in the GOBMs during the 1990s (open symbols) and 2000s (filled symbols) for the ocean regions used in Figures 3 and 4. Each symbol represents a single model as defined in Figure 3. Error bars (one standard deviation) are based on varying the end points of the trend calculation by ±1 year. All results are from the "climate only" simulation in order to focus on climate-driven trends.

Table S1. Spin-up procedure and climate forcing for global ocean biogeochemical models. Refer to Table A2 in the 2017 Global Carbon Budget (12) for additional model details.

Model	Spin-up procedure	Constant climate forcing	Variable climate forcing
CCSM-BEC (31)	Pre-spin-up of 740 years with CORE (32) normal-year forcing Additional spin-up using NCEP forcing 1958-2017	NCEP (33) forcing for year 1958	NCEP forcing 1958-2017
NorESM (34)	CORE normal year forcing for 1000 years	CORE normal year forcing	NCEP re-analysis with CORE-II corrections 1948-2016
NEMO-PlankTOM5 (35)	Initialization from GLODAP (36) plus 30-year spin-up under NCEP forcing from 1980	NCEP forcing 1980 repeated	NCEP forcing 1958-2017
CSIRO (37)	600-year spin-up using JRA-55 (38) pre-industrial forcing plus 2 cycles of JRA-55 from pre-industrial to 1957	JRA-55 forcing 1959 repeated	JRA forcing 1958-2016
MITgcm-REcoM-JRA (39)	2 cycles of JRA forcing (1958-2015)	JRA climatology (1958-2015)	JRA forcing 1958-2016
MITgcm-REcoM-NCEP (39)	48 years with CORE climatology	CORE climatology	NCEP forcing 1948-2016
NEMO-PISCES (CNRM) (40)	3000 years offline + 300 years online under NCEP forcing	NCEP forcing 1980 repeated	NCEP forcing 1948-2016
MPIOM-HAMOCC-GR15 (41) [1]	Pre spin-up of > 1000 years + additional spin-up with ERA-20C (42) forcing 1905-1930	ERA-20C forcing 1959 repeated	ERA-20C forcing 1930-2017
MPIOM-HAMOCC-TP04 (41) [2]	Pre spin-up of > 1000 years + additional spin-up with ERA-20C (42) forcing 1905-1930	ERA-20C forcing 1959 repeated	ERA-20C forcing 1930-2017

[1] Coarse-resolution version of the model, used in the 2017 Global Carbon Budget
[2] Finer-resolution eddy-permitting tripolar grid version of the model (41)

References

1. Ritter R, et al. (2017) Observation-Based Trends of the Southern Ocean Carbon Sink. *Geophysical Research Letters* 44(24):12–339.
2. Rödenbeck C, et al. (2015) Data-based estimates of the ocean carbon sink variability–first results of the Surface Ocean pCO2 Mapping intercomparison (SOCOM). *Biogeosciences* 12:7251–7278.
3. Jones SD, Le Quéré C, Rödenbeck C, Manning AC, Olsen A (2015) A statistical gap-filling method to interpolate global monthly surface ocean carbon dioxide data. *Journal of Advances in Modeling Earth Systems* 7(4):1554–1575.
4. Rödenbeck C, et al. (2014) Interannual sea–air CO_2 flux variability from an observation-driven ocean mixed-layer scheme. *Biogeosciences* 11:4599–4613.
5. Park GH, et al. (2010) Variability of global net sea–air CO2 fluxes over the last three decades using empirical relationships. *Tellus B: Chemical and Physical Meteorology* 62(5):352–368.
6. Iida Y, et al. (2015) Trends in pCO_2 and sea–air CO_2 flux over the global open oceans for the last two decades. *Journal of oceanography* 71(6):637–661.
7. Landschützer P, Gruber N, Bakker D, Schuster U (2014) Recent variability of the global ocean carbon sink. *Global Biogeochemical Cycles* 28(9):927–949.
8. Nakaoka S, et al. (2013) Estimating temporal and spatial variation of ocean surface pCO_2 in the North Pacific using a self-organizing map neural network technique. *Biogeosciences* 10(9):6093–6106.
9. Majkut JD, Sarmiento J, Rodgers K (2014) A growing oceanic carbon uptake: Results from an inversion study of surface pCO_2 data. *Global Biogeochemical Cycles* 28(4):335–351.
10. DeVries T (2014) The oceanic anthropogenic CO_2 sink: Storage, air-sea fluxes, and transports over the industrial era. *Global Biogeochemical Cycles* 28(7):631–647.
11. DeVries T, Holzer M, Primeau F (2017) Recent increase in oceanic carbon uptake driven by weaker upper-ocean overturning. *Nature* 542(7640):215.
12. Le Quéré C, et al. (2018) Global Carbon Budget 2017. *Earth System Science Data* 10(1):405–448.
13. Haverd V, et al. (2018) A new version of the CABLE land surface model (Subversion revision r4601) incorporating land use and land cover change, woody vegetation demography, and a novel optimisation-based approach to plant coordination of photosynthesis. *Geoscientific Model Development* 11(7).
14. Melton J, Arora V (2016) Competition between plant functional types in the Canadian Terrestrial Ecosystem Model (CTEM) v. 2.0. *Geoscientific Model Development* 9(1):323–361.
15. Oleson K, et al. (2013) Technical Description of version 4.5 of the Community Land Model (CLM).
16. Tian H, et al. (2015) North American terrestrial CO_2 uptake largely offset by CH_4 and N_2O emissions: toward a full accounting of the greenhouse gas budget. *Climatic Change* 129(3-4):413–426.
17. Jain AK, Meiyappan P, Song Y, House JI (2013) CO2 emissions from land-use change affected more by nitrogen cycle, than by the choice of land-cover data. *Global change biology* 19(9):2893–2906.
18. Reick C, Raddatz T, Brovkin V, Gayler V (2013) Representation of natural and anthropogenic land cover change in MPI-ESM. *Journal of Advances in Modeling Earth Systems* 5(3):459–482.
19. Clark D, et al. (2011) The Joint UK Land Environment Simulator (JULES), model description–Part 2: carbon fluxes and vegetation dynamics. *Geoscientific Model Development* 4(3):701–722.
20. Smith B, et al. (2014) Implications of incorporating N cycling and N limitations on primary production in an individual-based dynamic vegetation model. *Biogeosciences* 11:2027–2054.
21. Sitch S, et al. (2003) Evaluation of ecosystem dynamics, plant geography and terrestrial carbon cycling in the LPJ dynamic global vegetation model. *Global Change Biology* 9(2):161–185.
22. Keller KM, et al. (2017) 20th century changes in carbon isotopes and water-use efficiency: tree-ring-based evaluation of the CLM4. 5 and LPX-Bern models. *Biogeosciences (Online)* 14(10).
23. Zaehle S, Friend A (2010) Carbon and nitrogen cycle dynamics in the O-CN land surface model: 1. Model description, site-scale evaluation, and sensitivity to parameter estimates. *Global Biogeochemical Cycles* 24(1).
24. Krinner G, et al. (2005) A dynamic global vegetation model for studies of the coupled atmosphere-biosphere system. *Global Biogeochemical Cycles* 19(1).
25. Guimberteau M, et al. (2018) ORCHIDEE-MICT (v8. 4.1), a land surface model for the high latitudes: model description and validation. *Geoscientific Model Development* 11(1):121.
26. Woodward FI, Smith TM, Emanuel WR (1995) A global land primary productivity and phytogeography model. *Global biogeochemical cycles* 9(4):471–490.
27. Kato E, Kinoshita T, Ito A, Kawamiya M, Yamagata Y (2013) Evaluation of spatially explicit emission scenario of land-use change and biomass burning using a process-based biogeochemical model. *Journal of Land Use Science* 8(1):104–122.
28. Fay A, McKinley G (2014) Global open-ocean biomes: mean and temporal variability. *Earth System Science Data* 6(2):273–284.
29. Laufkotter C, et al. (2015) Drivers and uncertainties of future global marine primary production in marine ecosystem models. *Biogeosciences* 12(23):6955–6984.
30. Landschuetzer P, Gruber N, Bakker DC (2016) Decadal variations and trends of the global ocean carbon sink. *Global Biogeochemical Cycles* 30(10):1396–1417.
31. Doney SC, et al. (2009) Mechanisms governing interannual variability in upper-ocean inorganic carbon system and

air–sea CO_2 fluxes: Physical climate and atmospheric dust. *Deep Sea Research Part II: Topical Studies in Oceanography* 56(8-10):640–655.

32. Large WG, Yeager S (2009) The global climatology of an interannually varying air–sea flux data set. *Climate dynamics* 33(2-3):341–364.
33. Saha S, et al. (2014) The NCEP climate forecast system version 2. *Journal of Climate* 27(6):2185–2208.
34. Schwinger J, et al. (2016) Evaluation of NorESM-OC (versions 1 and 1.2), the ocean carbon-cycle stand-alone configuration of the Norwegian Earth System Model (NorESM1). *Geoscientific Model Development* 9:2589–2622.
35. Buitenhuis ET, Rivkin RB, Sailley S, Le Quéré C (2010) Biogeochemical fluxes through microzooplankton. *Global biogeochemical cycles* 24(4).
36. Key RM, et al. (2004) A global ocean carbon climatology: Results from Global Data Analysis Project (GLODAP). *Global biogeochemical cycles* 18(4).
37. Law RM, et al. (2017) The carbon cycle in the Australian Community Climate and Earth System Simulator (ACCESS-ESM1)–Part 1: Model description and pre-industrial simulation. *Geoscientific Model Development* 10(7):2567–2590.
38. Kobayashi S, et al. (2015) The JRA-55 reanalysis: General specifications and basic characteristics. *Journal of the Meteorological Society of Japan. Ser. II* 93(1):5–48.
39. Hauck J, Köhler P, Wolf-Gladrow D, Völker C (2016) Iron fertilisation and century-scale effects of open ocean dissolution of olivine in a simulated CO2 removal experiment. *Environmental Research Letters* 11(2):024007.
40. Séférian R, et al. (2013) Skill assessment of three earth system models with common marine biogeochemistry. *Climate Dynamics* 40(9-10):2549–2573.
41. Ilyina T, et al. (2013) Global ocean biogeochemistry model HAMOCC: Model architecture and performance as component of the MPI-Earth system model in different CMIP5 experimental realizations. *Journal of Advances in Modeling Earth Systems* 5(2):287–315.
42. Poli P, et al. (2016) ERA-20C: An atmospheric reanalysis of the twentieth century. *Journal of Climate* 29(11):4083–4097.